A. Supplementary material: Sensitivity analysis

The present sensitivity analysis provides a better understanding of the mechanisms that may affect the dynamics of the granular column collapse when some of the soil properties or numerical parameters are deliberately modified.

A.1. K_1 sensitivity

Figure 9 displays the influence of K_1 values on the collapse dynamics. We observe relatively small differences between $K_1 = 40$ and $K_1 = 100$ due to the dilatancy coefficient (δ) restricted to the range $-0.4 \leq \delta \leq 0.4$. After the gate removal, both $K_1 = 40$ and $K_1 = 100$ scenarios reach the limit $|\delta| = 0.4$ in some regions of the granular column, thus, no relevant difference is observed between $K_1 = 40$ and $K_1 = 100$. As we approach the equilibrium state, δ values decay suppressing the dilatancy effect, though in the $K_1 = 100$ case, dilatancy effects are mildly higher during the $\phi \rightarrow \phi_\infty$ transition.

The loose case displayed in figure 9 shows K_1 has a stronger effect on the dynamics of the spreading deposit. Large K_1 values enhance a rapid flow with longer run-out distances because positive pore pressure develops within the granular medium (see the positive pressure jumps in figure 9) reducing the shear strength of the system.

Figure 9 also shows a case where the limit of the dilatancy coefficient is set to $|\delta| = 5$. This scenario predicts the correct positive overshoot of pore pressure for the initially loose column but dilatancy effects fluidize a significant region of the granular column, which leads to a deposit shape that resembles a horizontal sediment layer. Regarding the dense case, the negative pore pressure is overpredicted, the expansion of the granular column occurs extremely rapid, so dilatancy effects go from an immediate large impact to an irrelevant contribution in the early stages. This results in a granular collapse that flows normally without dilatancy effects. At this point, it is worth noting that in most of literature (Pailha et al., 2009; Mutabaruka et al., 2014), the dilatancy prefactor K_1 is found to be in the range of $K_1 \in [1 - 50]$.

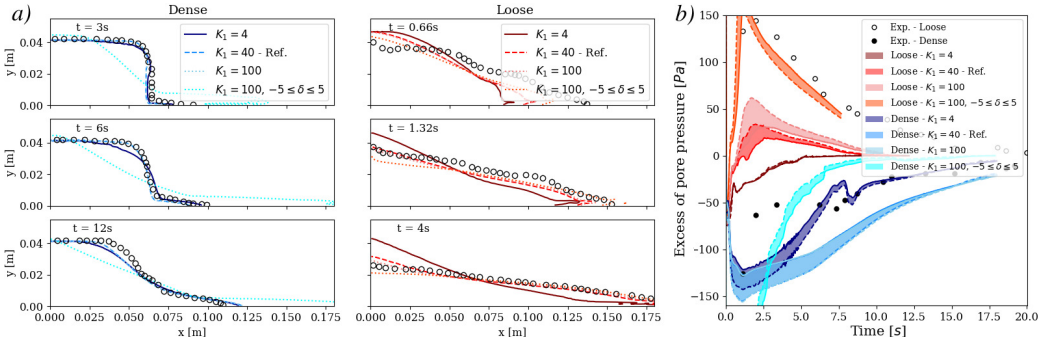

Figure 9. *Evolution of the morphology during the collapse of an initially dense and loose columns. b) Evolution of basal pore pressure measured at 2cm (− continuous line) and 3cm (−− dashed line). Shady areas correspond to the region between the two probes results. The influence of K_1 is investigated.*

One may think, following the logic of the dilatancy model presented in this work, that the pore pressure jump is higher because we are enhancing a rapid granular flow accompanied with contractancy, thus, a reduction of the pore space that results in positive pore pressure. However, the pressure jump is not only influenced by this transition, instead, the dynamics of the sliding failure and spreading are even more important. The fact that the shear strength is reduced more rapidly with increasing K_1 displaces the failure line quickly and the non-moving zone (where zero or negative pore pressures are observed - see figure 4b) is getting smaller much faster. The consequences of this mechanism are a more elongated

bed, as more granular material is mobilized, and positive pore pressures measured at the probe location which is now placed under the sliding region.

A.2. ϕ_c sensitivity

The influence of the critical volume fraction (ϕ_c) is displayed in figure 10. By changing the value of the critical volume fraction one can adjust the dilatancy effects. Eq. 15 and Eq. 17 show dilatancy effects are proportional to $\phi - \phi_c/(1 + I_v^{1/2})$. Therefore, as shown in figure 10, lower ϕ_c values result in lower contractancy effects for initially loose cases (the gap $\phi - \phi_c/(1+I_v^{1/2})$ is reduced) and stronger dilatancy effects for initially dense packings (the gap $\phi - \phi_c/(1+I_v^{1/2})$ is increased). Likewise, larger ϕ_c values are associated to weaker dilatancy in dense cases and enhanced contractancy for loose granular columns. Changes in ϕ_c are remarkably more important in the loose packings. Indeed, contractancy effects can fluidize a significant region of the granular column, which leads to a deposit shape closer to a horizontal sediment layer. Correspondingly, the pore pressure dynamics are significantly higher for the loose case. In particular, the $\phi_c = 0.58$ case reproduces the magnitude of the positive pore pressure jump reported in the experiments. On the contrary, minor differences in terms of pore pressure are observed for initially dense columns.

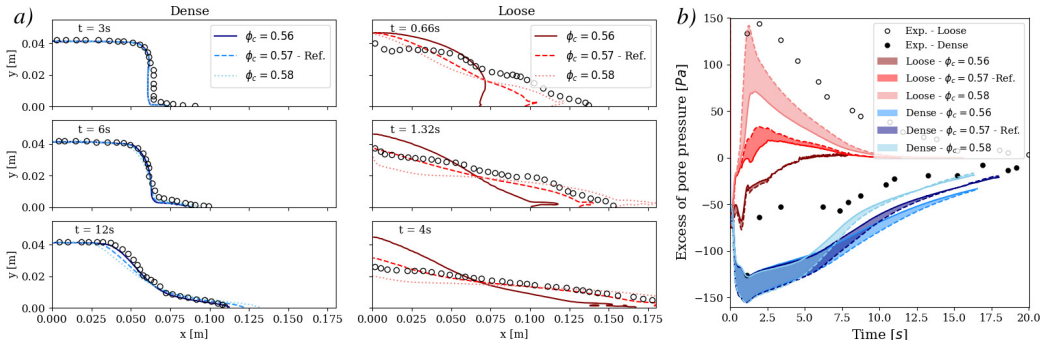

Figure 10. *Evolution of the morphology during the collapse of an initially dense and loose columns. b) Evolution of basal pore pressure measured at 2cm (− continuous line) and 3cm (−− dashed line). Shady areas correspond to the region between the two probes results. The influence of ϕ_c is investigated.*

A.3. K_2 sensitivity

Figure 11 illustrates the negligible effect of K_2 on the dynamics of the granular column collapse. The shear-induced pressure remains residual and the collapse is controlled by changes in the contact pressure. Besides, the dense collapse simulation conducted using $K_2 = 1$ evidences undesirable numerical fluctuations that compromise the accuracy of the results, thus, additional relaxation is required to complete the numerical simulations with satisfactory results.

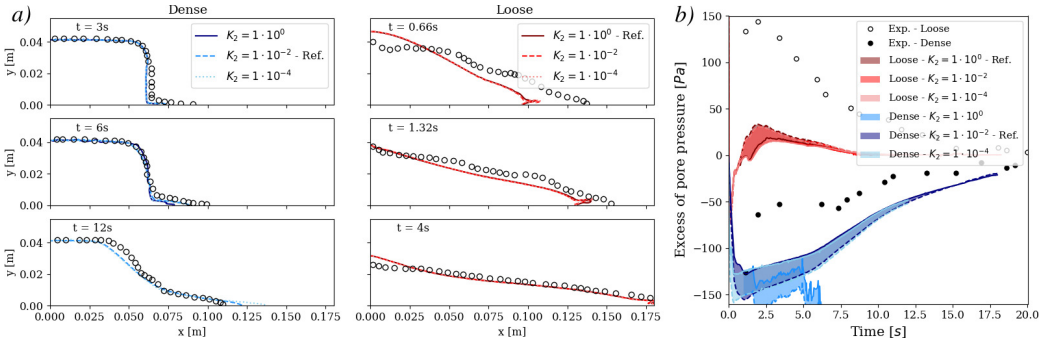

Figure 11. *Evolution of the morphology during the collapse of an initially dense and loose columns. b) Evolution of basal pore pressure measured at 2cm (− continuous line) and 3cm (−− dashed line). Shady areas correspond to the region between the two probes results. The influence of K_2 is investigated.*

A.4. Influence of elastic modulus

Figure 12 shows profiles and pore pressure curves for two different elastic modulus (E) exhibiting limited differences. However, these differences are not solely due to the stiffness of the soil, but rather the different vertical concentration profiles that result from using various elastic modulus. Indeed, figure 13 provides evidence that using different elastic modulus values leads to different initial concentration profiles after the sedimentation.

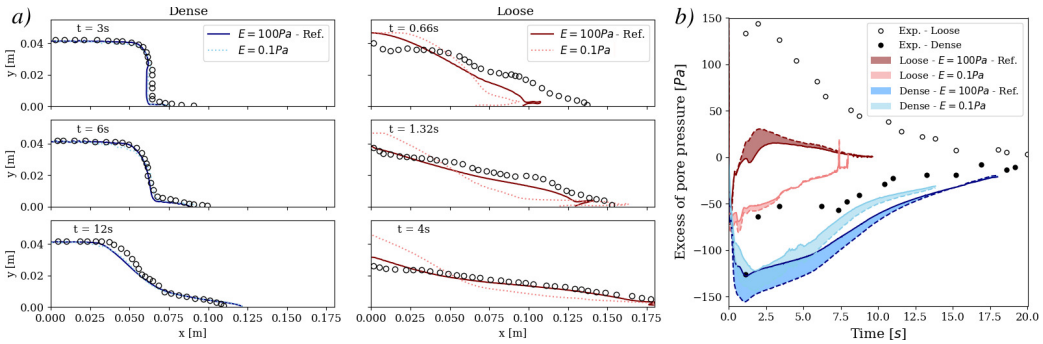

Figure 12. *Evolution of the morphology during the collapse of an initially dense and loose columns. b) Evolution of basal pore pressure measured at 2cm (− continuous line) and 3cm (−− dashed line). Shady areas correspond to the region between the two probes results. The influence of E is investigated.*

The solid volume fraction is determined after the sedimentation process, where granular material settles under its own weight. Since we use an expression to model the granular pressure based on the volume fraction (see Eq. 12), once the sedimentation is complete, the weight of the granular layer is balanced by the contact pressure. This implies that we obtain a lithostatic granular pressure, which can only be achieved with a non-constant volume fraction profile. High values of E result in steep concentration profiles, which are more realistic. However, numerical instabilities arise when E exceeds $100Pa$. It is worth noting that for $E = 100Pa$, very small changes in the volume fraction are observed between the top and bottom of the granular layer. As a consequence of the non-uniform vertical concentration profile, the upper regions tend to behave as a looser material than the layers located below. This behavior is accentuated for the loose case with $E = 0.1Pa$ (see figures 12 and 13) where the difference in the initial concentration between the top and bottom granular layer is around $\Delta\phi = \phi_{bottom} - \phi_{top} \approx 0.04$. Therefore, it is unsurprising that the pore pressure values registered at the

bottom for the loose case using $E = 0.1Pa$ are shifted downwards (only negative values are predicted) because that region is denser than the one corresponding to the $E = 100Pa$ case.

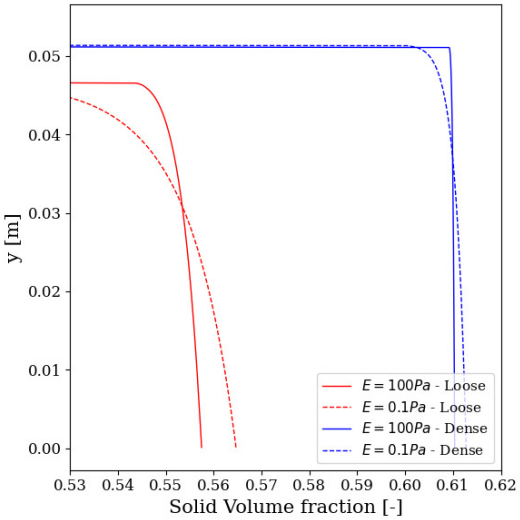

Figure 13. *Vertical concentrations profiles at the middle of the granular column ($x = L_o/2$) using different elastic modulus.*

A.5. Influence of permeability

In order to study the role of permeability, Engelund's coefficients in Eq. 5 are increased to lower the permeability of the granular material. More precisely, $\alpha_E = 1500$ and $\beta_E = 780$ are considered. Figure 14 shows lower permeabilities lead to a slow mobilization. In turns, the pressure dissipation takes longer as expected. Furthermore, figure 14 suggests different Engelund's coefficients have a negligible impact on the results for the loose granular column regarding the morphology and the pore pressure curve.

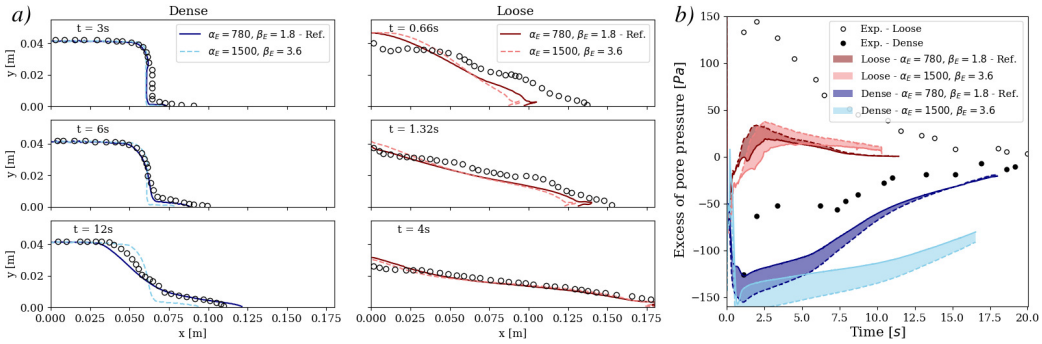

Figure 14. *Evolution of the morphology during the collapse of an initially dense and loose columns. b) Evolution of basal pore pressure measured at 2cm (− continuous line) and 3cm (−− dashed line). Shady areas correspond to the region between the two probes results. The influence of Engelund's coefficients is investigated.*

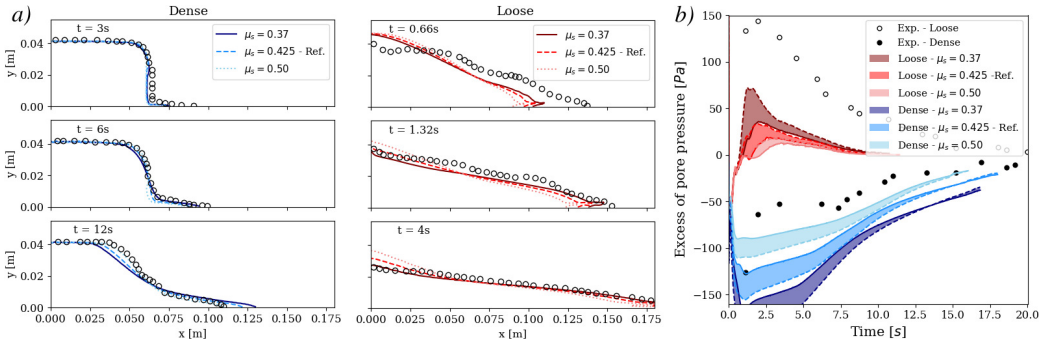

Figure 15. *Evolution of the morphology during the collapse of an initially dense and loose columns. b) Evolution of basal pore pressure measured at 2cm (− continuous line) and 3cm (−− dashed line). Shady areas correspond to the region between the two probes results. Different rheological coefficients are considered.*

A.6. Rheological coefficients

Figure 15 shows large friction coefficients delay the collapse and, at the end of the simulation, the deposit is characterized by a steeper slope. The lower mobilization entails a weaker pore pressure feedback: the soil is more difficult to shear, thus, pore volume changes take longer. On the contrary, figure 15 indicates low fiction angles enhance a rapid failure with abrupt pore volume changes, therefore, higher pore pressure jumps are observed for both initially dense and loose granular columns.

B. Supplementary material: Mesh convergence test

Adopting different mesh sizes in the numerical model has a strong influence on the accuracy of the results. In this analysis, three mesh sizes are considered. Figure 16a shows the amount of rounding observed at the top of the breach wall is highly dependent on the grid size, with more rounding observed for larger grid cells and sharper corners for finer meshes. The time series displayed in figure 16a also evidences an increment of the wall velocity as grid cells become larger. Finally, figure 16b shows larger pressure jumps are predicted as the grid size increases. Moreover, pore pressure is dissipated more rapidly for coarser meshes. The same pattern was reported by Weij et al. (2020). The mesh refinement study displayed in figure 16 is not converged, however, finer meshes render the computation unfeasible for realistic simulations. In spite of the evident discrepancies in the pore pressure curves observed in figure 16b, the shape of the deposit and the wall velocity show reasonable differences between the $\Delta x/D_{50} = 20.8$ and the $\Delta x/D_{50} = 10.4$ grid sizes.

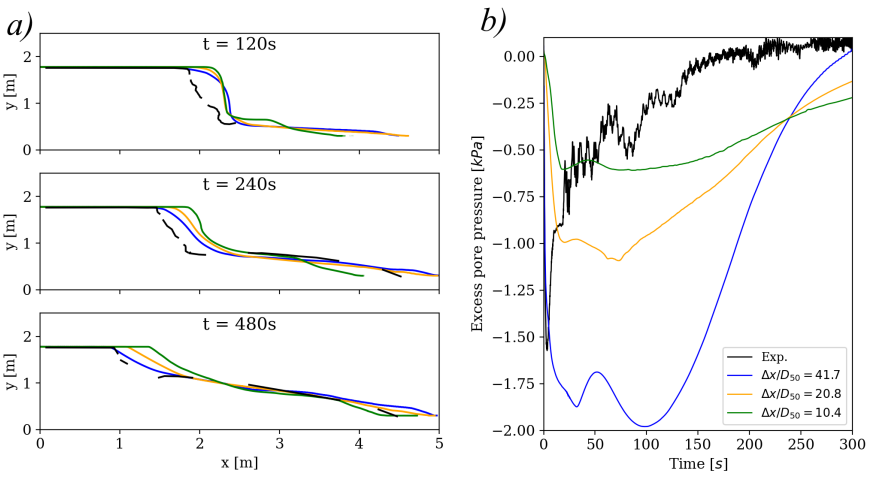

Figure 16. *a) Comparison of the morphology and b) pore pressure (p^f) evolution within the granular column between the experiments and the numerical simulations for the GEBA sand. Three mesh sizes are considered.*